

Rapid intensity decrease during the second half of the first millennium BCE in Central Asia and global implications

Raquel Bonilla Alba, Myriam Gómez-paccard, F. J Pavón-carrasco, J. Del Del Río, E. Beamud, V. Martínez-ferreras, J. M Gurt-esparraguera, E. Ariño-gil, A. Palencia-ortas, F. Martín-hernández, et al.

▶ **To cite this version:**

Raquel Bonilla Alba, Myriam Gómez-paccard, F. J Pavón-carrasco, J. Del Del Río, E. Beamud, et al.. Rapid intensity decrease during the second half of the first millennium BCE in Central Asia and global implications. Journal of Geophysical Research : Solid Earth, 2021, 126 (10), pp.e2021JB022011. 10.1029/2021jb022011 . insu-03388201

HAL Id: insu-03388201
https://insu.hal.science/insu-03388201

Submitted on 20 Oct 2021

HAL is a multi-disciplinary open access archive for the deposit and dissemination of scientific research documents, whether they are published or not. The documents may come from teaching and research institutions in France or abroad, or from public or private research centers.

L'archive ouverte pluridisciplinaire **HAL**, est destinée au dépôt et à la diffusion de documents scientifiques de niveau recherche, publiés ou non, émanant des établissements d'enseignement et de recherche français ou étrangers, des laboratoires publics ou privés.

Check for updates

Accepted Article

Rapid intensity decrease during the second half of the first millennium BCE in Central Asia and global implications

R. Bonilla-Alba[1,2*], M. Gómez-Paccard[2], F. J. Pavón-Carrasco[1], J. del Río[2], E. Beamud[3], V. Martínez-Ferreras[4], J. M. Gurt-Esparraguera[4], E. Ariño-Gil[5], A. Palencia-Ortas[1,2], F. Martín-Hernández[1,2], A. Chauvin[6], M. L. Osete[1,2]

[1] Department of Physics of the Earth and Astrophysics, Complutense University of Madrid (UCM), Avd. Complutense s/n, 28040-Madrid, Spain.

[2] Institute of Geosciences IGEO (CSIC-UCM), Spanish National Research Council, c/ del Doctor Severo Ochoa 7, Edificio Entrepabellones 7 y 8, 28040, Madrid, Spain.

[3] Paleomagnetic Laboratory CCiTUB-Geo3Bcn, Geosciences Barcelona CSIC, C/ Lluís Solé i Sabarís s/n, 08028, Barcelona, Spain

[4] ERAAUB, Department of Ancient History and Archaeology, University of Barcelona, Carrer de Montalegre, 6-8, 08001 Barcelona, Spain

[5] Department of Prehistory, Ancient History and Archaeology, University of Salamanca, C/ Cervantes s/n, 37002, Salamanca, Spain

[6] Univ Rennes, CNRS, Géosciences-Rennes - UMR 6118, F-35000, Rennes, France.

*Corresponding author: Raquel Bonilla-Alba (raquelbo@ucm.es)

Key Points:

1. We present 51 new TRM-anisotropy corrected archeointensities for South Uzbekistan.

2. An important decrease in intensity is observed between 400 BCE and 100 BCE – 1 CE, probably associated with non-dipolar sources.

3. Similar intensity V-shaped trends are observed at continental scale.

This article has been accepted for publication and undergone full peer review but has not been through the copyediting, typesetting, pagination and proofreading process, which may lead to differences between this version and the Version of Record. Please cite this article as doi: 10.1029/2021JB022011.

This article is protected by copyright. All rights reserved.

Abstract

Recent paleomagnetic studies have shown that important short-lived intensity fluctuations occurred during the first millennium BCE. However, the knowledge of the spatial and temporal extension of these features is still limited by the scarce availability of robust data. In this study we focus on the study of the intensity decrease that took place in Central Asia during the second half of the 1st millennium BCE after the high intensities that characterized the Levantine Iron Age Anomaly. Since previous archeointensities available for this period and region were obtained without accomplishing modern standards of quality, we present here new archeointensities that are derived from classical Thellier and Thellier experiments, including partial thermoremanent magnetization (pTRM) checks, thermoremanent magnetization (TRM) anisotropy and cooling rate corrections at the specimen level. The new 51 archeointensities, together with previous archeointensities, have been used to present a new local paleosecular variation curve for Central Asia. The results confirm the existence of an important geomagnetic field intensity decrease in South Uzbekistan from the 4th century BCE to the end of the 1st century BCE associated with rates of changes up to -15 μT/century. A critical analysis of the archeointensity global database indicates that this feature was present at continental scale, from Western Europe to Central Asia. However, this trend is not identified in other regions such as Japan or Mexico. Finally, the comparison with the dipole moment derived from recent global geomagnetic field reconstructions suggests a strong influence of non-dipolar sources upon this continental intensity feature.

Plain Language Summary

The Earth’s magnetic field (also called the geomagnetic field) is continuously changing over time and space. Since the 19th century, the behavior of the geomagnetic field is known through direct observations performed in geomagnetic observatories and satellites. However, the only way to recover past geomagnetic field in ancient times is through paleomagnetic and archeomagnetic studies. In particular, archeomagnetism is the study of heated archeological materials, which include ferromagnetic particles acting as a compass and recording the geomagnetic field direction and strength at a certain time. When the archeological material cools down the ferromagnetic particles save the direction and intensity, like a photograph of the ancient geomagnetic field. Nowadays, there are very few archeomagnetic studies dealing with archeological materials from Central Asia. In this work, we present the variation of the geomagnetic field intensity between 600 BCE - 600 CE in Uzbekistan deduced from a complete archeomagnetic investigation of 70 pottery fragments. The results confirm a rapid variation of geomagnetic field strength between 400 BCE and 100 BCE-1CE. To determine the spatial expression of this feature we compared the obtained trend for Central Asia with the geomagnetic field intensity evolution in other regions of the world.

Keywords: archeomagnetism; archeointensity; secular variation; South Uzbekistan; Central Asia

1 Introduction

The geomagnetic field measured at the Earth’s surface is the result of various sources. The main field, generated in the outer core, has changed over time at different time scales, varying from years (geomagnetic jerks) to tens of thousands of years (reversals or excursions). The temporal variation of the main geomagnetic field at timescales of years

to centuries and beyond is known as secular variation and brings us information about the dynamics of the outer core. In spatial terms, the main field is the result of two contributions: the dipole field that explains the 90% of the total field at the Earth's surface and the non-dipole fields with about the 10% of contribution.

Since the middle of the 19th century, the spatial and temporal evolution of the main geomagnetic field is well known though the instrumental data. However, the only way to decipher past geomagnetic field changes before the era of direct measurements comes from the paleomagnetic study of the remanent magnetization acquired by the iron oxides present in certain rocks and baked archeological materials and retained over historical or geological time scales. This magnetization can be analyzed in the paleomagnetic laboratories to infer the direction and strength of the ancient geomagnetic field. Since past changes of the geomagnetic field observed at the Earth's surface are not equal throughout the world due to the different contributions of dipolar and non-dipolar sources at each location, in order to have a global view of the past geomagnetic field it is necessary to investigate its behavior at different regions.

Strong variations in geomagnetic field intensity occurred during the first millennium BCE. Extremely high paleointensities were first reported by Ben-Yosef et al. (2009) and Shaar et al. (2011) from the archeointensity study of Jordanian and Israelian copper slags dated around 1000 BCE. Later studies confirmed these anomalous high strength field values in the Levant and surrounding regions (e.g., Ertepinar et al., 2012, 2020; Shaar et al., 2016, 2017; Ben-Yosef et al., 2017). Shaar et al. (2016) named this high intensity feature observed in the Levant from about 1050 BCE to 700 BCE as the Levantine Iron Age Anomaly (LIAA). Rapid changes in geomagnetic field strength during the first

millennium BCE have also been reported in other parts of the world: Canary Islands (de Groot et al., 2015; Kissel et al., 2015), the Azores Archipelago (Di Chiara, et al., 2014), Western and Central Europe (Hervé et al., 2013, 2017; Molina-Cardín et al., 2018; Osete et al., 2020; Schnepp et al., 2020), the Mediterranean area (Béguin et al., 2019; Rivero-Montero et al., 2021a), eastern and central China (Cai et al., 2017, 2020), Korea (Hong et al., 2013) and Texas, USA (Bourne et al., 2016). The youngest intensity maxima in the European region for the first millennium BCE occurred around 500 BCE (Rivero-Montero et al., 2021a). After 500 BCE, the strong field vanished and a subsequent time interval characterized by a decreasing trend of geomagnetic field strength was observed over the Mediterranean area (Rivero-Montero et al., 2021a). To further investigate if this behavior is also observed eastwards, we present here the archeointensity and rock-magnetic study of 70 pottery fragments from Southern Uzbekistan (Central Asia). The new data, together with a critical revision of previous results, provide an improved vision of the geomagnetic field intensity changes in the region between 600 BCE and 600 CE. The present study is the first step of a long-term project which aims to decipher geomagnetic field strength changes in Central Asia over the past few millennia and that will complement the recently published archeointensity results from Bukhara (Uzbekistan) dated between the end of the 16th century and the beginning of the 19th century (Troyano et al., 2021).

2 Archeological contexts

The ceramic assemblages studied were collected in three archeological sites located in Bactria: Kurganzol (KGZ), Kampyr Tepe (KPT) and Termez (TRZ). This historical

region is comprised by the current territories of southern Uzbekistan, Tajikistan, and northern Afghanistan (see Fig. 1 and supporting information for further details).

[Insert Figure 1]

2.1 Archeological sites and dating constraints

Archaeological data suggest that the three investigated sites were founded during or shortly after Alexander the Great's campaigns in ancient Bactria (late 4th century BCE). The relative chronologies proposed for each site are based on numismatics and the techno-typological analysis of the ceramic wares, tracing parallels with other well-dated coeval sites in Bactria. All ^{14}C and techno-typological dates available, with calibrated calendar years and probability percentages for 1σ and 2σ, are listed in Table S1. In the present study, the dating assigned to each pottery sample was based on the typological chronology and the ^{14}C data when available, and was specified by considering the presence of coins, the chronologies determined to each unit of the stratigraphic sequence and the chronologies proposed to the same ceramic prototypes and types in other regional archaeological sites.

The first site, Kurganzol, was excavated by the Institute of Fine Arts of the Academy of Sciences of Uzbekistan in 2008. It lies at 924 meters a.s.l. (above sea level), in the southern foothills of the Hissar Range (current Uzbekistan), and on the southern bank of the Uchkul river, a tributary of the Surkhan Darya. Kurganzol consists of a circular fortress, about 35 meters in diameter, surrounded by a thick wall made with mud bricks, with several defensive towers attached to its north-eastern side. The archaeological context and absolute dating (dendrochronology) suggest a date for the occupation

sequence which should be established in the late 4th century BCE – beginning of the 3rd century BCE (Sverchkov, 2013, see supporting information for details).

The second site, Kampyr Tepe, comprises a citadel and a dwelling area in the fluvial terrace, which included a river moat. The materials investigated here were recovered from different archaeological contexts: the citadel, the low city, and a pottery workshop (see Martínez Ferreras et al., 2016 and supporting information for details). The pottery workshop includes two circular kilns that were excavated in the eastern sector outside the walls which have been dated by typological dating between late 4th BCE and 1st century BCE. Several small firing structures were also found in the eastern side of the citadel (Bolelov, 2001, 2011). ^{14}C analysis carried out at the Radiocarbon Dating Laboratory of the University of Barcelona on charcoal from one of these firing structures from citadel dates its use between the late 4th and mid-2nd century BCE. Also, ^{14}C absolute dating has been performed on materials from the low city which dated from 2nd to first half of the 1st century BCE.

Termez was settled close to the mouth of the Surkhan Darya, a tributary of the Amu Darya. It has systematically been excavated since the 1990s; one of the most active archaeological research teams from the last decades is the Uzbek-Spanish team IPAEB, led by the University of Barcelona and the Institute of Fine Arts of Uzbekistan. The city developed from the original fortress, the citadel, was built probably by the successors of Alexander in Seleucid times (first half of the 3rd century BCE) (Martínez Ferreras et al., 2019). It was extended during the Greco-Bactrian (mid-3rd to mid/late-2nd century BCE), Yuezhi (mid/late 2nd century and 1st century BCE) and Kushan periods (1st to mid-3rd centuries CE), becoming an important Buddhist center. The materials for this study were

recovered from two different areas. The sherds dated in the Yuezhi/early Kushan nomadic period come from the sector AC located in the alluvial plain. The fortress of Tchingiz Tepe provides materials dated in the Kushan and Kushano-Sasanian sequence. Radiocarbon analysis has been performed at the Radiocarbon Dating Laboratory of the University of Barcelona and the National Center of Accelerators in Seville on vegetable charcoal and bone found in several strata of the two settlements. The results suggest an occupation between the late-3rd century BCE and the 1st century CE for the alluvial plain. The materials from Tchingiz Tepe here studied are dated between the 2nd and the 4th centuries CE (Martínez Ferreras et al., 2014, 2019 and supporting information for details).

2.2 Materials: the tableware of ancient Bactria

The chemical, mineralogical and petrographic composition of the studied collection was characterized in previous studies (Gurt et al., 2015; Martínez Ferreras et al., 2016, 2019) by using an ensemble of archeometric techniques, including WD-XRF (Wavelength Dispersive X-Ray Fluorescence), XRD (X-Ray Diffraction), SEM-EDS (Scanning Electron Microscope with Energy Dispersive X-Ray Spectroscopy), and thin section optical microscopy. These studies prove that the chemical variability is very low between the ceramic vessels found in the same site, suggesting the use of very similar raw materials and therefore, a common local/regional origin. The variability detected is frequently explained by the use of different technological processes in the pottery manufacture (mainly in the processing of the clayey paste) and the development of secondary minerals due to weathering processes.

The materials used in this study (see Fig. 1) are fine-to-medium-grained calcareous pottery fragments, fairly homogeneous in their composition but with distinctive

inclusions depending on their provenance and their intended use. The ceramic wares from the alluvial plain (Kampyr Tepe and Termez) show non-plastic inclusions consisting of fragments of igneous and metamorphic rocks, together with crystals derived from granitoids (mainly quartz, feldspar and phyllosilicates); fragments and crystals of volcanic effusive rocks are scarce. By contrast, pottery from Kurganzol exhibits finer non-plastic inclusions consisting of the same lithology, although crystals and fragments of volcanic rocks are rare or absent, being a distinctive finding in the vessels from the Amu Darya basin. Since Kampyr Tepe comprised at least two pottery workshops dated to the Hellenistic and probably Greco-Bactrian periods, the provenance of most of the tableware analyzed from this site has been determined as local (Martínez Ferreras et al., 2016). In contrast, no workshop has been excavated from either in Kurganzol nor in Termez. It is highly unlikely that pottery was produced in the former military fortress, and therefore the vessels from Kurganzol have been considered as regional products. Moreover, the compositional differences detected among these samples and those found at Kampyr Tepe and Termez reveal that they were not produced in the Amu Darya floodplain. At Termez, all the samples analyzed were recovered from the alluvial plain (sectors AC1 and AC2) and have been considered as local/regional products (Martínez Ferreras et al., 2019). In contrast, for the tableware from the Tchingiz Tepe, dated to the Kushan and Kushano-Sasanian periods, a local provenance has been established (Gurt et al., 2015). It should be noted that Termez was an important ceramic production centre during the Kushan and probably the Kushano-Sasanian period, as attested by several pottery kilns associated with the Buddhist communities (Martínez et al. 2014; Tsantini et al. 2016).

3 Methods

Each pottery sherd (sample) selected for archeomagnetic analysis was sub-divided into different specimens-per-sample, yielding a total of 175 specimens that underwent experimental procedures. Specimens were named and marked, weighed, and encased in 2.2 cm^3 quartz cubes, using a mix of glass wool and sodium silicate to prevent their moving during the heating and measuring stages. The rock-magnetism and paleointensity experiments were carried out at the paleomagnetic laboratories of the Complutense University of Madrid (Spain) and Géosciences-Rennes (Univ. Rennes, CNRS, UMR 6118, France).

3.1 Rock-Magnetic experiments

Susceptibility versus temperature (χ-T) curves were carried out for a total of 29 samples using a Kappabridge KLY-4 susceptibility meter coupled to a CS4 furnace (AGICO). This device increases the temperature progressively and measures the bulk susceptibility of the powdered sample in each step. In this study, the temperature was increased from room temperature to 700°C, and then cooled back to room temperature in an Ar atmosphere. In addition, 28 saturation magnetization versus temperature (Ms-T) curves were done in a Variable Field Translation Balance (VFTB) (Mag-Instruments, Petersen and Petersen, 2008). Magnetization was measured in an applied field of 1 T warming up to around 650ºC and further cooling back to 40ºC in air. These experiments can be used to estimate the Curie/Néel temperature of the magnetic minerals contained in our samples, and to check for thermally induced magnetic alteration by comparing the heating and cooling branches of the plots. From the Ms-T curves we calculated the corresponding Curie/Néel temperatures following the second derivative method proposed by Tauxe

(1998) to find the inflection points and convexities of the curves. This was done with the RockMagAnalyzer 1.1 software (Leonhardt, 2006).

Hysteresis loops, isothermal remanent magnetization (IRM) acquisition curves and further direct current IRM demagnetization or back field saturation IRM (SIRM) curves were performed in 53 samples using a J-Meter Coercivity-Spectrometer, originally designed at Kazan federal University's paleomagnetism laboratory and improved by Jasonov et al. (1998). This instrument consists of a non-magnetic wheel, 50 cm in diameter, which rotates 18 times per second through an electromagnet. The in-field magnetic remanence of the sample, which is secured in a holder on the outer rim of the wheel, is measured while the electromagnetic field increases up to 500 mT and then decreases to the opposite polarity (-500 mT). The hysteresis loops, after calculation and subtraction of the paramagnetic contribution, were used to calculate the saturation magnetization (M_s), the saturation remanent magnetization (M_{rs}), the coercive field (H_c). The remanent coercive field (H_{cr}) associated with the samples is derived from the back-field IRM curves. The hysteresis parameters have been classically plotted in the so-called Day diagram, that was specifically designed to estimate the domain state of magnetite/titanomagnetite bearing rocks (Day et al., 1977) and where the magnetization parameters ratio (M_{rs}/M_s) is plotted against the coercivity parameters ratio (H_{cr}/H_c). We also plotted in this diagram the SD-MD mixing curves for magnetite (Dunlop, 2002). However, as noted by Roberts et al. (2018), the use of the Day plot to infer the domain state of the samples should be discarded. We have therefore only used the Day plot to identify anomalous samples in our collection. The shape of the hysteresis cycles can also be used to identify samples containing two or more magnetic populations with different coercivities, usually associated with wasp-waisted hysteresis loops (Tauxe, 1998). For this purpose, coercivity spectra of the IRM acquisition curves were analyzed using the

model proposed by Kruiver et al. (2001) to determine the number and properties of the magnetic components. We also calculate the saturation IRM and the median destructive field at which half of the SIRM is reached. To do this a curve fitting of the IRM vs the logarithm of the applied field is done using three different approaches: linear scale (LAP), gradient (GAP) and probability scale (SAP). Here we obtained, for the majority of the samples, the best fit of the IRM curves considering three magnetic components but for some specific cases it was necessary to also consider a 4^{th} and 5^{th} components, but being these components related with less than 10% of the total content. The component related to the lowest coercivity has been interpreted as a thermal activation of the magnetic particles and therefore neglected for further interpretation (Heslop et al., 2004).

Finally, in order to determine the existence of a single or multiple natural remanent magnetization (NRM) components we performed alternating field (AF) demagnetization experiments of the initial NRM over 30 pottery fragments, using a 2G cryogenic SQUID (Superconducting Quantum Interference Device) magnetometer. These experiments have been performed up to maximum fields of 120 mT in two different cycles, the first one from 0 to 40 mT with progressive steps of 5 mT; and the second one with steps of 20 mT, from 40 to 120 mT.

3.2 Paleointensity experiments

To estimate the past geomagnetic field strength, we applied the classical Thellier-Thellier method (Thellier & Thellier 1959), including partial thermoremanent magnetization (pTRM) checks, and the thermoremanent magnetization (TRM) anisotropy and cooling rate corrections upon intensity estimates. The magnetization was measured with a 2G SQUID magnetometer. Sample heating was performed in a Thermal Demagnetizer

MMTD-24 (Magnetic Measurements) and the locally-manufactured "Ramsés" furnace at Géosciences-Rennes. The temperature was progressively raised from 100ºC to 530-560ºC in 10-11 steps, each step consisting of two heating and cooling cycles with an applied field of 50 μT along the *Z* axis of the samples: first in +*Z*, then in the opposite way. In order to check the thermal stability of the samples we measured the susceptibility after each temperature step with a MS3 susceptibility meter (Bartington Instruments), and performed pTRM checks every two steps of temperature. The effect of the TRM anisotropy on paleointensity determinations was calculated by measuring the acquisition of TRM in 6 different directions (±X, ±Y, ±Z) at a heating step for which around the 70% of the NRM is lost. In addition, and in order to check the TRM anisotropy protocol applied we decided to place sister specimens from one fragment (TRZ302) in three different faces of the cubes (denoted as specimens B, C and L in Table S2; see also Osete et al., 2016 for a similar experiment). Finally, the cooling rate correction factors were calculated following the method described in Gómez-Paccard et al. (2006 and 2008) after the TRM anisotropy determination or at the end of paleointensity experiments (when around 85-95% of the NRM was lost). For this, we heated the samples at the same temperature in 4 different steps: the first two steps were made in the usual way, that is to say, during the first step the sample was heated during 45 minutes with the magnetic field applied in +Z direction and after cooled in about 45 minutes with the same magnetic field; in the second step the duration of the heating and cooling is the same as for the first step, but the magnetic field was applied in –Z direction. In order to determine the variation of the TRM acquisition, on the third step the sample was heated during 45 minutes with the magnetic field applied in +Z direction but the time to cool off was 24 hours; at the end of this additional cycle the samples are heated in –Z direction and the cooling is done in about 45 minutes. Comparing the third and first step we can calculate the effect of the cooling

rate upon TRM acquisition capacity. Thanks to the second and fourth steps we can control potential changes in the TRM acquisition capacity related to thermally induced mineralogical changes. If the mineralogical evolution during the cooling rate is higher than the effect the cooling rate, this correction is not considered.

4 Results

4.1 Rock-magnetic characterization

In order to identify the principal magnetic minerals responsible for the magnetization different rock-magnetism experiments have been performed (see section 3.1). The majority of the thermomagnetic curves performed are almost reversible, which points to no significant magnetic alteration during the thermal treatment of the samples (Figs. 2a and 2b). This indicates that the studied samples might be promising for successful paleointensity determination. The Curie temperatures (Fig. 2a) obtained range between 269 and 640ºC corresponding to different magnetic carriers. According to the results we divided our collection in two groups. The first group (including 15 samples, 55.6%) presents two different Curie temperatures: one at low temperatures, ranging from 269 to 380ºC, which could be related to maghemite shells around magnetite cores (O´Reilly, 1984); another one is observed at high temperatures between 553 and 635ºC which can be related to either magnetite or maghemite. At this stage we cannot distinguish between these minerals, with quite similar values for the Curie/Néel temperatures 580°C (magnetite) and 610°C (maghemite) due to the large error in Curie temperature determination and linked to the smoothed Ms-T curves obtained. The second group (11 samples, 40.7%) corresponds to a single Curie temperature, ranging between 545 and

604ºC, pointing to magnetite or maghemite as the principal magnetic carriers. Also, one exception has been identified, the sample TRZ595 shows two phases corresponding to titanomagnetites with different Ti content (T_c=481ºC) and magnetite (T_c=561ºC). In Fig. 2b one representative χ-T thermomagnetic curve per studied city is represented. In these plots we can visually ascertain a peak between 300-400ºC, which could be associated with maghemite shells around magnetite cores. This observation seems to be consistent with the phenomenon and shapes observed by O´Reilly (1984) and mentioned earlier.

[Insert Figure 2]

Hysteresis loops were used to calculate the hysteresis parameters (Fig. 2c). M_s varies between 0.024 - 0.520 Am^2/kg and M_r between 0.190 – 0.003 Am^2/kg. H_c ranges between 13.5 – 2.2 mT and saturation is reached at 150 mT, suggesting the presence of low-coercivity minerals. H_{cr} varies between 47.0 – 14.0 mT. The hysteresis ratios obtained are presented in a Day plot (Day, 1977), modified as proposed by Dunlop (2002) to see where our samples lay in the theoretical PSD-SD (pseudo-single domain PSD / single domain SD) regions for magnetite, including magnetite mixing (Fig. 2d). As commonly observed in other archeointensity studies (e.g. Gómez-Paccard et al., 2012a, 2019; Rivero-Montero et al., 2021b), most of the samples fall in the PSD region. No SP content was detected by using J-coercivity measurements, which can be used to estimate SP existence with the decay of the SIRM when reversing the field (Jasonov et al., 1998). Therefore, it is very likely that the displacement towards higher values of the Hcr/Hc ratio could be related to some maghemitization of the samples. This effect is also observed for the two outliers from Kampyr Tepe which fall close to the MD (multi-domain) range. These two samples

(TRZ554 and TRZ230) present high coercivity values which might indicate the presence of maghemite or hematite.

IRM acquisition up to 500 mT (Fig. 2e and Fig. S1 from the supporting information) were measured and the coercivity component analysis proposed by Kruiver et al. (2001) was performed. These experiments confirm the presence of a main low-coercivity fraction (1st component) with a median destructive field of about 30 mT, which contributes to 70-80% of the total magnetization. The second component contributes to 10-20% and corresponds to a median destructive field of about 70 mT. Finally, the third component, corresponding to around 5-10% shows a very low median destructive field (of about 5 mT) that can be associated with thermal activation of the magnetic particles (see Heslop et al., 2004). These results suggest that the magnetite or titanomagnetite particles contained in our samples are close to the single domain state, ideal conditions to carry out successful paleointensity experiments. Finally, AF demagnetization of the NRM had been performed using sister specimens. Almost all the samples have a single component of magnetization which is completely demagnetized at 120 mT (see a typical example in Fig. 2f). These results confirm the rock magnetic results previously described. In summary, rock magnetic analysis indicates that the principal magnetic carriers in our ceramic assemblage probably are low Ti-content magnetite, magnetite and/or maghemite.

4.2 New paleointensity data for Uzbekistan

A total of 175 specimens from 70 different fragments were prepared and measured. In Fig. 3 representative Arai plots are presented. For paleointensity determination, in some cases we discarded the first steps of temperature (100-200ºC) which correspond to a

viscous component. Samples were completely demagnetized at temperatures between 480 and 560ºC. In order to ensure the reliability of paleointensity determinations, we used common quality criteria similar than those used in our previous publications (e.g., Gómez-Paccard et al., 2012b, 2016). The paleointensities have been only calculated for specimens that corresponded to a single component of magnetization with a straight line pointing to the origin in the Zijderveld plots and linear Arai diagrams (Figs. 3 a-j). The maximum difference accepted between pTRM checks ant the original TRMs obtained at the same temperature step was 10%, this criterion was also applied for pTRM anisotropy checks. The fraction of the TRM used to determinate the paleointensity data, f parameter (Coe et al., 1978) should be at least 50% and 5 or more temperature steps must be used to determinate the slope. Following Shaar et al. (2016) we have considered a maximum value of 5º and 10º for the angular deviation MAD (Kirschvink, 1980) and the deviation angle DANG (Tauxe & Staudigel, 2004), respectively. It is worth noting that we have accepted a single specimen (KPT2229) with a MAD value slightly higher than 5º because all the other parameters are correct, and the intensity value obtained is very similar to the values obtained for the other two sister specimens studied (see Table S2). In addition, this high MAD value seems to be related to an anomalous high noise level in one single step rather than to a bad magnetic behaviour. Around 74% (129 from 175) of the studied specimens have been retained for paleointensity determination.

[Insert Figure 3]

In Fig. 4, the different parameters used to evaluate the quality of the paleointensity estimates are showed. The fraction of the NRM used to calculate the paleointensity data

ranges between 0.54 and 0.95. The quality factor q (Coe et al., 1978) varies between 10.2 and 115.9. The curvature parameter k (Paterson, 2011) and the ratio of the standard error of the slope to the absolute value f the slope (β ratio) range between 0.01 and 0.836 and between 0.0063 and 0.0466, respectively, although these parameters were not used as rejection criteria. As indicated before the highest MAD value obtained is 5.3º for one single specimen, being all the other values lower than 5º with a minimum of 0.8º. DANG values range between 0.2º and 3.3º. Thanks to the applied criteria we consider that the paleointensity estimates proposed can be considered as highly reliable.

[Insert Figure 4]

The influence of TRM anisotropy and cooling rate on paleointensity determinations has been largely recognized. Here we analyse these effects at the specimen level. Important differences (up to 30%) are found between the uncorrected and TRM anisotropy corrected intensities (see supporting information online). These results agree with previous archeomagnetic studies where very important differences have been obtained between the uncorrected and corrected intensities when pottery fragments are studied (e.g., Osete et al., 2016; Gómez-Paccard et al., 2019). In order to check the TRM anisotropy protocol applied we decided to place sister specimens from the Termez collection in different faces of the cubes. In general, specimens named with the letters A or B were placed in the central part of the base of the quartz cubes. Specimens denoted as C were placed perpendicular to the base of the cube and, finally, in some cases a third sister specimen, denoted as L, was placed in one of the lateral faces of the quartz cubes. It can be seen in Table S2 how very different intensity values are obtained before and after the TRM

correction, especially for the Termez collection. The standard deviations (s.d) of the means are substantially reduced after the TRM anisotropy correction (see Table S2). For example, the s.d. for the fragment TRZ364 was 10.5 μT before the correction and 0.7 μT after. Concerning the cooling rate experiments, the corrections factors obtained (see supporting information) range between 0.7 and 11.3%, with a mean value of about 5%. This is in agreement with recent results obtained for archeomagnetic materials (Hervé et al., 2019a).

From the paleointensity determinations obtained at the specimen level (Table S2) we have derived 51 mean paleointensities: 11 calculated from 4 specimens, 13 from 3 specimens, 19 from 2 and 9 from just one single specimen (see Table 1). The more specimens we use, the greater statistical confidence on the mean value we have. Therefore, and following our recent publications (Osete et al., 2020; Rivero-Montero et al., 2021a), we classified our new data in two categories. The first one (called high-quality paleointensities) corresponds to data derived from three specimens and the lower quality group includes the other data obtained from 1 or 2 specimens. It is worth noting that since the main objective of this paper is to detect the rapid variations of the geomagnetic field, we decided to not calculate a mean value for the different age groups given in Table 1 since some of them are associated with large age uncertainties.

[Insert Table 1]

To have a global view of the geomagnetic field strength variations in our targeted area, the new mean intensities were relocated to Termez coordinates (37.3ºN, 67.2ºE) using the virtual axial geomagnetic pole (Fig. 5). The general trend described by our new collection suggests a V-shaped behavior of geomagnetic field strength in South Uzbekistan between 300 BCE and 200 CE. The new high-quality paleointensity results obtained in this study (calculated from 3 or more specimens, Table 1) suggest that the intensity of the geomagnetic field was much higher around 300 BCE than around 200 BCE where the lowest high-quality values are observed (see big dots in Fig. 5) indicating fast intensity changes at multidecadal scales. Moreover, the new high-quality determinations derived from the well-dated site of Kurganzol (310 –290 BCE, orange dots in Fig. 5) suggest a large geomagnetic field strength variation (between 66.6 and 51.5 μT, in situ coordinates) at decadal scales. Therefore, the new data evidence a rapid intensity decrease in South Uzbekistan around 300 BCE. In Kampyr Tepe (blue dots in Fig. 5), a total of 22 new intensities have been obtained dated between the end of 310 BCE and 100 BCE, with in general lower values than those obtained for Kurganzol, specially for the group of fragments from the pottery workshop (2d in Table 1). The high-quality paleointensities obtained for Kampyr Tepe range between 62.1 and 38.4 μT (in situ coordinates). However, the large age uncertainties associated with this collection makes it difficult to infer a detailed description about multidecadal intensity changes during this period. In Termez (purple dots in Fig. 5), samples from 6 different age groups have given successful results, but only one of them corresponds to a high-quality intensity (fragment TRZ302 derived from 3 specimens). The 2 results obtained for the oldest group (3a in Table 1) indicate a variation between 47.6 and 41.9 μT during the 3rd century BCE. The results obtained for the stratigraphic unit AC1 - SU 12 (group 3b) indicate a range of the intensity between 45.6 μT and 38.7 between 100 BCE and 100 CE. Finally, the mean value obtained for

Tchingiz Tepe samples (groups 3c-f, 100-350 CE) of about 50 ± 4 μT further support a higher geomagnetic field intensity around this time, in comparison with our BCE collection. However, it is necessary to investigate more well-dated fragments in order to better describe geomagnetic field intensity features around the targeted periods.

5 Discussion

5.1 A new paleointensity secular variation curve for Uzbekistan between 600 BCE and 600 CE.

The new mean intensities are compared in Fig. 5 with previous paleointensity results from archeological sites located within a radius of 1000 km around Termez and corresponding to the period 600 BCE – 600 CE. As with the new data, the previous dataset was also relocated to the Termez coordinates. The number of the previous studies is significant and 72 paleointensities derived from the study of bricks, potteries or baked materials (Burlatskaya et al., 1995; Nachasova and Burakov, 1994, 1996, 1997). These older data were obtained with the Thellier and Thellier intensity method (1959) but, in case of Burlatskaya et al., (1995), without considering the TRM anisotropy effect upon paleointensity estimations. The importance of this effect on potteries has been recognized since several decades (e.g., Rogers et al., 1979) and it is now accepted that this correction needs to be performed at the specimen level. If not considered the real past intensity field values can be erroneously estimated with potential errors up to 90% (e.g., Genevey et al., 2008; Osete et al., 2016; Gómez-Paccard et al., 2012b, 2019). In this study, for example, differences up to 30% between the uncorrected and corrected values are obtained (see see

supporting information). Moreover, the cooling rate effect upon intensity estimates was also not considered in these studies. In a recent work, Hervé et al. (2019a) have studied the influence of cooling rate in a set of 35 baked bricks and concluded that, on average, the non-corrected results overestimated the expected value by 5-6%. These values are of the same order of magnitude as the mean correction proposed by Genevey et al. (2008) from an analysis of the global database. In our studied collection cooling rate factors up to 12% have been obtained with a mean value for the overall collection of 5% in agreement with the results obtained by Hervé et al. (2019a) and Genevey et al. (2008). Therefore, another potential source of error can be identified in the ancient data available for the targeted region. In order to consider this effect and in agreement with the studies cited before, a 5% reduction in the paleointensity estimates have been applied for the previous intensities available.

[Insert Figure 5]

As it can be seen in Figure 5 new and previous data are quite consistent, although some discrepancies can also be observed. As discussed before, the reliability of the data cannot be considered as equal, and we decided to classify the data in three different categories using an appropriate weighting scheme designed for this purpose. Data obtained with 3 or more specimens and including the TRM and cooling rate corrections and pTRM checks were considered as the most reliable group and a weight of 10 was used. Data with TRM anisotropy and cooling rate corrections and pTRM checks but obtained with less than 3 specimens were assigned to an intermediate weight of 5 and, finally, the other data were considered as the less reliable group with an associated weight of 1. We calculated a new paleointensity paleosecular variation (PSV) curve for Central Asia using the compiled

dataset together with the new results (shown in Fig. 5) and using the mentioned weights. To fit the paleointensity data to a time-continuous curve we applied the same approach than Rivero-Montero et al. (2021a). In summary, this method provides an ensemble of 5,000 PSV curves by bootstrapping the paleointensity data in both age and intensity domains (including the error estimations). In addition, to obtain a more robust PSV curve, we eliminate possible outliers by detecting the data which residuals (the difference between data and curve) are 3 times higher than the root mean square error of the curve fitting. Only one data point has been identified as an outlier, data around 485 BCE (Burlatskaya et al., 1995), (see Table S3 from the supporting information for more details). The mean and the standard deviation (1σ or 2σ) of the ensemble of 5,000 PSV curves provide the final PSV curve for South Uzbekistan. The new local PSV curve obtained (Fig. 5) shows an intensity maximum around 400 BCE followed by a rapid decrease of about −15 μT/century until 100 BCE. However, we must notice that this maximum is constrained by some archeointensity values higher than 80 μT that are included in the less reliable group, suggesting that this intensity bump might not reflect a real feature of the past geomagnetic field. New quality data covering this time interval are needed to confirm this hypothesis. The curve also shows an intensity minimum value around 100 BCE followed by a slowly growing trend until 500 CE. Finally, the compiled dataset has been compared with global paleomagnetic reconstructions: SHA.DIF.14k (Pavón-Carrasco et al., 2014), ARCH10k.1 and CALS10k.2 (Constable et al., 2016) and the SHAWQ family models (Campuzano et al., 2019; Osete et al., 2020). Results show notable discrepancies between data and model estimations. In detail, the models do not reproduce the minima and maxima values reported by the data and the intensity decrease observed in the 1st millennium BCE is much less pronounced in all these paleoreconstructions. These discrepancies (quantified for some time periods up to 15 μT) point out the need to obtain more quality data in the

region to develop new and improved paleomagnetic reconstructions, and also emphasizing the importance of well-established local paleosecular variation curves.

5.2 Comparison with neighboring regions and global implications

To analyze if intensity changes in Uzbekistan are reflecting global or regional patterns of the past geomagnetic field, we have compared the virtual axial dipole moment (VADM) directly calculated from the data and the dipole moment (DM) and Axial Dipole Moment (ADM) derived from the global reconstructions previously mentioned. As shown in Fig. 6 the VADMs exhibit much stronger fluctuations than the global ADM-DM, showing higher values between 600 and 300 BCE and lower estimations from 200 BCE to 300 CE. This suggests an important regional geomagnetic field behavior due to the non-dipolar contributions.

[Insert Figure 6]

In order to investigate if similar geomagnetic field intensity trends are observed in other regions, we used the complete global database from 600 BCE – 600 CE (GEOMAGIA50V3.4 database, Brown et al., 2015 updated with recent publications: García-Redondo et al., 2020; Rivero-Montero et al., 2021a) to compile the VADM values available for different regions (1000 km of radius, see Fig. 7). The results are plotted from west to east in Fig. 7. In Mexico, a VADM maximum of $16 \cdot 10^{22}$ Am^2 can be seen around 200 BCE but this feature is only based on two high-quality values (Hervé et al., 2019b). Nevertheless, this maximum is not observed in Peru, where high-quality data seem to present a minimum of VADM around this age. Moving to Europe, a maximum of $17 \cdot 10^{22}$ Am^2 is observed around 500-450 BCE followed by a decreasing trend until 100 BCE in

Western Europe (Osete et al., 2020), Germany (Hervé et al., 2013, 2017; Schnepp et al., 2020), Italy and Greece (Tema & Lanos, 2021; Rivero-Montero et al., 2021a), the Caucasian region and the Levant (Shaar et al., 2017). Moving eastwards, in Central Asia, we also observe a VADM maximum around 400 BCE in Uzbekistan, around one century later than in Western Europe, but this maximum is based on low quality data that do not accomplish modern standard criteria of quality. In India, and due to the low number of data, a maximum cannot be clearly identified, but a decreasing tendency is also observed during the second half of the 1st millennium BCE. A similar V-shape trend is observed from Western Europe to India, with the minima values between 100 BCE and 200 CE. In Eastern Asia and Japan (Cai et al., 2017, 2020; Hong et al. 2013), there is no evidence of a maximum around 500-400 BCE if the high-quality dataset is considered, but some high VADM values of low quality are present in China. It is, however, hard to define a clear tendency in these areas due to the important dispersion of the corresponding regional databases.

[Insert Figure 7]

We also calculated the PSV curves obtained from the different regional datasets (see supporting information) following the methodology described before, using the mentioned categories of high- and low- quality data and different weights for each category, giving weights from 1 to 10 depending on the quality of the data. From this, the intensity secular variation rates (μT/century) have been calculated in 100-year time windows. The results, presented in Fig. 8, showed a very similar trend all over Europe. The maximum variation (9.6 μT/century) is observed in Western Europe (Iberia and

France-Germany) between 400 BCE and 300 BCE. This maximum variation is lower eastwards where values of 3.3 μT/century are obtained for the Caucasus between 200 BCE and 100 BCE. In Central Asia, the maximum values (14.7 μT/century) are achieved in Uzbekistan between 400 and 300 BCE, at the same time as in Western Europe. However, in the Levant and India the maximum variation is around three times lower than in Uzbekistan and appears between 300-100 BCE. As is mentioned previously, these rapid changes are not observed in Eastern Asia and the Americas.

[Insert Figure 8]

The maximum rate of change obtained for Uzbekistan is similar to the one associated with the sharp intensity decrease recently identified between 1560 and 1725 in the same region (Troyano et al., 2020). It is, however, significantly lower than the rates of change of about 75-150 μT/century proposed for the LIAA (Ben-Yosef et al., 2017; Shaar et al., 2016). It is worth noting that the rates of changes proposed here are derived from PSV smoothed curves and therefore the maximum rates of change are most probably underestimated. This highlights the need to obtain a more detailed description of the past changes of geomagnetic field strength at the decadal scale. Finally, our results suggest a similar V-shape behaviour for the intensity element (i.e., a maximum around 500-400 BCE followed by a rapid decrease) in a large region of more than 7000 km from Western Europe (5ºW longitude) to central Asia (80ºE longitude). This wavelength on the surface of the Earth is equivalent to a spherical harmonic of degree n = 5-6, which is compatible with a non-dipolar source of the Earth´s magnetic field generated in the outer core.

6 Conclusions

Fifty-one new paleointensity data, at the sample level, have been obtained for South Uzbekistan with ages ranging between 310 BCE and 300 CE, a period for which no high-quality paleointensity data were previously available. Our new results provide evidence of a rapid drop in intensity during the second half of the 1st millennium BCE showing a minimum of about 30 μT around 200 BCE – 1 CE. Together with previous archeointensities our results allow us to present a new local PSV curve for Central Asia. The results suggest a V-shaped intensity behaviour in Central Asia during the 600 BCE up to 600 CE period. High-intensity field values around 400 BCE were achieved in Uzbekistan followed by a sharp decrease until 100 BCE - 1 CE associated with rates of changes of about −15 μT/century. A progressive recovery of geomagnetic field strength is then observed during the first centuries of the CE. This behaviour is also observed at the continental scale, from Western and Central Europe to the Levant and Central Asia but cannot be detected eastwards in areas such as China and Japan or the Americas, although the low number of high-quality intensity data from this last continent hamper some more meaningful analysis. The important differences observed between the VADMs values available for Uzbekistan and the DM (ADM) estimations derived from different global geomagnetic field paleoreconstructions suggest the strong influence of non-dipolar sources upon this continental feature.

Acknowledgements and Data Statement

Financial support was given by the Spanish Ministry of Science and Innovation thorough the projects CERAC (HAR2016-75133-C3-1-P), CONCERAC (HAR2016-75133-C3-3-P) and SPYKE (CGL2017-87015-P). RBA thanks the FPI fellowship (PRE2018-085949)

associated with the SPYKE project. This study has been also funded by the Ramón y Cajal program (contracts of MGP and VMF, refs. RYC-2013-14405 and RYC-2014-15789). The authors wish to acknowledge the professional support of the CSIC Interdisciplinary Thematic Platform Open Heritage: Research and Society (PTI-PAIS). EB thanks the Geomodels Research Institute (UB) and the Grup de Geodinàmica i Anàlisi de Conques -2017SGR596 (Generalitat de Catalunya). APO thanks the PTA contract of the Spanish Ministry of Science and Innovation. Special thanks to S. Pidaev from the Academy of Sciences of the Republic of Uzbekistan for its great help during the sampling campaign in Uzbekistan. We also thank our colleagues from the palaeomagnetism group of Madrid, especially S.A. Campuzano and E. Delso, and the great archeological team that helped us during the archeomagnetic field campaigns in Uzbekistan. The data that support the findings of this study are openly available in MagIC (10.7288/V4/MAGIC/19307) and GEOMAGIA (https://geomagia.gfz-potsdam.de/). Additional information upon request to raquelbo@ucm.es or mgomezpaccard@csic.es. The Editor, Mark Dekkers and reviewers, Lisa Tauxe and Evdokia Tema are sincerely acknowledged for their constructive comments on our manuscript.

Supporting Information

Supporting information related to this article can be found online.

References

Baumer, C. (2012). *The History of Central Asia: The Age of the Steppe Warriors (Volume 1)*. London: I.B. Tauris & Co Ltd.

Béguin, A., Filippidi, A., de Lange, G. J., & de Groot, L. V. (2019). The evolution of the Levantine Iron Age geomagnetic Anomaly captured in Mediterranean sediments.

Earth and Planetary Science Letters, *511*, 55-66. doi.org/10.1016/j.epsl.2019.01.021

Ben-Yosef, E., Tauxe, L., Levy, T. E., Shaar, R., Ron, H., & Najjar, M. (2009). Geomagnetic intensity spike recorded in high resolution slag deposit in Southern Jordan. *Earth and Planetary Science Letters*, *287*(3-4), 529-539. https://doi.org/10.1016/j.epsl.2009.09.001.

Ben-Yosef, E., Millman, M., Shaar, R., Tauxe, L., & Lipschits, O. (2017). Six centuries of geomagnetic intensity variations recorded by royal Judean stamped jar handles. *Proceedings of the National Academy of Sciences*, *114*(9), 2160-2165.. doi.org/10.1073/pnas.1615797114

Bolelov, S. B. (2001). Goncharnaya masterskaya III–II vekov do ne na Kampyrtepa. *Materialy Toharistanskoj jekspedicii*, *2*, 15-30.

Bolelov, S. B. (2011). Proizvodstvyennyy tsyentr epokhi Ellinizma na Tsitadyeli Kampyrtepa. *Matyerialy Tokharistanskoy Ekspyeditsii. Arkhyeologichyeskiye isslyedovaniya Kampyrtepa*, *8*, 48-79.

Bourne, M.D., Feinberg, J.M., Stafford, T.W., Waters, M.R., Lundelius, E., & Forman, S.L. (2016). High-intensity geomagnetic field "spike" observed at ca. 3000 cal BP in Texas, USA. *Earth and Planetary Science Letters*, 442, 80–92. doi.org/10.1016/j.epsl.2016.02.051

Brown, M. C., Donadini, F., Korte, M., Nilsson, A., Korhonen, K., Lodge, A., Lengyel, S.N. & Constable, C. G. (2015). GEOMAGIA50. v3: 1. General structure and modifications to the archeological and volcanic database. *Earth, Planets and Space*, *67*(1), 1-31. doi.org/10.1186/s40623-015-0232-0

Burlatskaya, S., Lykov, A. & Chernykh, I. (1995). Geomagnetic field variations in Central Asia for the last 4000 years. *Izvestiya, Physics of the Solid Earth*, 31, 407–

416.

Cai, S., Jin, G., Tauxe, L., Deng, C., Qin, H., Pan, Y., & Zhu, R. (2017). Archaeointensity results spanning the past 6 kiloyears from eastern China and implications for extreme behaviors of the geomagnetic field. *Proceedings of the National Academy of Sciences, 14*(1), 39-44. doi.org/10.1073/pnas.1616976114

Cai, S., Tauxe, L., Wang, W., Deng, C., Pan, Y., Yang, L., & Qin, H. (2020). High-fidelity archeointensity results for the Late Neolithic Period from Central China. *Geophysical Research Letters,* 47, e2020GL087625. doi.org/10.1029/2020GL087625.

Campuzano, S.A., Gómez-Paccard, M., Pavón-Carrasco, F.J., & Osete, M.L. (2019). Emergence and evolution of the South Atlantic Anomaly revealed by the new paleomagnetic reconstruction SHWQ2k. *Earth and Planetary Science Letters,* 512, 17-26. doi.org/10.1016/j.epsl.2019.01.050

Coe, R.S., Grommé, C.S., & Mankinen, E.A. (1978). Geomagnetic paleointensities from radiocarbon-dated lava flows on Hawaii and the question of the Pacific nondipole low. *Journal of Geophysical Research: Solid Earth*, *83*(B4), 1740-1756. doi.org/10.1029/JB083iB04p01740

Constable, C., Korte, M., & Panovska, S. (2016). Persistent high paleosecular variation activity in southern hemisphere for at least 10 000 years. *Earth and Planetary Science Letters*, *453*, 78-86. doi.org/10.1016/j.epsl.2016.08.015

Day, R., Fuller, M., & Schmidt, V.A. (1977). Hysteresis properties of titanomagnetites: Grain-size and compositional dependence. *Physics of the Earth and planetary interiors, 13*(4), 260-267. doi.org/10.1016/0031-9201(77)90108-X

de Groot, L.V., Béguin, A., Kosters, M.E., Rijsingen, E.M. Van, Struijk, E.L.M., Biggin, A.J., Hurst, E.A., Langereis, C.G., & Dekkers, M.J. (2015). High paleointensities

for the Canary Islands constrain the Levant geomagnetic high. *Earth and Planetary Science Letters*, 419, 154–167. doi.org/10.1016/j.epsl.2015.03.020

di Chiara, A., Tauxe, L., & Speranza, F. (2014). Paleointensity determination from São Miguel (Azores Archipelago) over the last 3 ka. *Physics of the Earth and planetary interiors*, 234, 1–13. doi.org/10.1016/J.PEPI.2014.06.008

Dunlop, D.J. (2002). Theory and application of the Day plot (Mrs/Ms versus Hcr/Hc) 1. Theoretical curves and tests using titanomagnetite data. *Journal of Geophysical Research: Solid Earth*, *107*(B3), EPM-4. doi.org/10.1029/2001JB000486

Ertepinar, P., Langereis, C.G., Biggin, A.J., Frangipane, M., Matney, T., Ökse, T., & Engin, A. (2012). Archaeomagnetic study of five mounds from Upper Mesopotamia between 2500 and 700 BCE: Further evidence for an extremely strong geomagnetic field ca. 3000 years ago. *Earth and Planetary Science Letters*, 357–358, 84–98. doi.org/10.1016/J.EPSL.2012.08.039

Ertepinar, P., Hammond, M.L., Hill, M.J., Biggin, A.J., Langereis, C., Herries, A.I.R., Yener, K., Akar, M., Gates, M.-H., Harrison, T., Greaves, A., Frankel, D., Webb, J.M., Özgen, İ., & Yazicioglu, G.B. (2020). Extreme geomagnetic field variability indicated by Eastern Mediterranean full-vector archaeomagnetic records. *Earth and Planetary Science Letters*, 531, 115979. doi.org/10.1016/j.epsl.2019.115979

Genevey, A., Gallet, Constable, C. G., Korte, M. & Hulot, G. (2008). ArcheoInt: An Upgraded Compilation of Geomagnetic Field Intensity Data for the Past Ten Millennia and Its Application to the Recovery of the Past Dipole Moment. *Geochemistry, Geophysics, Geosystems*, 9, Q04038. doi.org/10.1029/2007GC001881

García-Redondo, N., Calvo-Rathert, M., Carrancho, A., & Bustamante-Álvarez, M. (2020). New high precision full-vector archaeomagnetic data from a roman kiln in

Mérida (Spain). *Physics of the Earth and Planetary Interiors*, *309*, 106591. doi.org/10.1016/j.pepi.2020.106591

Gómez-Paccard, M., Chauvin, A., Lanos, P., Thiriot, J., & Jiménez-Castillo, P. (2006). Archeomagnetic study of seven contemporaneous kilns from Murcia (Spain). *Physics of the Earth and Planetary Interiors*, *157*(1-2), 16-32. doi.org/10.1016/j.pepi.2006.03.001

Gómez-Paccard, M., Chauvin, A., Lanos, P., Thiriot J. (2008). New archeointensity data from Spain and the geomagnetic dipole moment in western Europe over the past 2000 years, *Journal of Geophysical Research*, 113, B09103, doi:10.1029/2008JB005582.

Gómez-Paccard, M., McIntosh, G., Chauvin, A., Beamud, E., Pavón-Carrasco, F.J., & Thiriot, J. (2012a). Archeomagnetic and rock magnetic study of six kilns from North Africa (Tunisia and Morocco). *Geophysical Journal International*, *189*, 169-186. doi.org/10.1111/j.1365-246X.2011.05335.x

Gómez-Paccard, M., Chauvin, A., Lanos, P., Dufresne, P., Kovacheva, M., Hill, M. J., Beamud, E., Blain, S., Bouvier, A., Guibert, P., & Archaeological Working Team (2012b). Improving our knowledge of rapid geomagnetic field intensity changes observed in Europe between 200 and 1400 AD. *Earth and Planetary Science Letters*, *355*, 131-143. doi.org/10.1016/j.epsl.2012.08.037

Gómez-Paccard, M., Osete, M.L., Chauvin, A., Pavón-Carrasco, F.J., Pérez-Asensio, M., Jiménez, P., & Lanos, P. (2016). New constraints on the most significant paleointensity change in Western Europe over the last two millennia. A non-dipolar origin? *Earth and Planetary Science Letters*, *454*, 55-64. doi.org/10.1016/j.epsl.2016.08.024

Gómez-Paccard, M., Chauvin, A., Albeck, M.E., Zaburlín, M. A., Basso, D. M., Pavón-Carrasco, F.J., Osete, M.L., & Campuzano, S.A. (2019). New archeointensity data from NW Argentina (1300–1500 CE). *Physics of the Earth and Planetary Interiors*, 286, 92-100. doi.org/10.1016/j.pepi.2018.11.004

Gurt Esparraguera, J.M., Ariño Gil, E., Martínez Ferreras, V., & Pidaev, Sh.R. (2015). The Buddhist occupation of Tchingiz Tepe (Termez, Uzbekistan) in the Kushan period through the ceramic contexts. *Archaeological Research in Asia*, 3, 19–33. doi.org/10.1016/j.ara.2015.04.003

Hervé, G., Chauvin, A., & Lanos, P. (2013). Geomagnetic field variations in Western Europe from 1500 BC to 200 AD. Part II: New intensity secular variation curve. *Physics of the Earth and Planetary Interiors*, 218, 51–65. doi.org/10.1016/J.PEPI.2013.02.003

Hervé, G., Faβbinder, J., Gilder, S.A., Faβbinder, J., Metzner-Nebelsick, C., Geisweid, L., Reuβ, S., Flontas, A., Walter, F., Westhausen, I., Gallet, Y., Genevey, A., Schnepp, E., Pütz, A., Wittenborn, F., Linke, R., & Riedel, G. (2017). Fast geomagnetic field intensity variations between 1400 and 400 BCE: New archaeointensity data from Germany. *Physics of the Earth and Planetary Interiors*, 270, 143–156. doi.org/10.1016/j.pepi.2017.07.002

Hervé, G., Chauvin, A., Lanos, P., Rochette, P., Perrin, M., & d´Arc, M.P. (2019a). Cooling rate effect on thermoremanent magnetization in archaeological baked clays: an experimental study on modern bricks. *Geophysical Journal International*, *217*(2), 1413-1424. doi.org/10.1093/gji/ggz076

Hervé, G., Perrin, M., Alva-Valdivia, L.M., Rodríguez-Trejo, A., Hernández-Cardona, A., Córdova-Tello, M., & Meza-Rodríguez, C. (2019b). Secular variation of the intensity of the geomagnetic field in Mexico during the first millennium BCE.

Geochemistry, Geophysics, Geosystems, 20(12), 6066-6077. doi.org/10.1029/2019GC008668

Heslop, D., McIntosh, G., & Dekkers, M. J. (2004). Using time- and temperature-dependent Preisach models to investigate the limitations of modelling isothermal remanent magnetization acquisition curves with cumulative log Gaussian funtions. *Geophysical Journal International,* 157(1), 55–63. doi.org/10.1111/j.1365-246X.2004.02155.x

Heußner, K.U., & Boroffka, N. (2013). Dendrochronological and Radiocarbon dating of samples om Kurganzol (Uzbekistan), in L.M. Sverchkov, Kurganzol. *Kurganzol-Krepost Aleksandra na yugye Uzbekistana.* Tashkent, Uzbekistan: SMI-ASIA. pp. 182-184.

Hong, H., Yu, Y., Hee, C., Hee, R., Park, J., Doh, S., Kim, W., & Sung, H. (2013). Globally strong geomagnetic field intensity circa 3000 years ago. *Earth and Planetary Science Letters*, *383*, 142-152. doi.org/10.1016/j.epsl.2013.09.043

Jasonov, P. G., Nougaliev, D. K., Burov, B. V. & Heller, F. (1998). A modernized coercivity spectrometer. *Geologica Carpathica*, 49(3), 224-225.

Kirschvink, J.L. (1980). The least-squares line and plane and the analysis of paleomagnetic data. *Geophysical Journal International*, *62*(3), 699-718. doi.org/10.1111/j.1365-246X.1980.tb02601.x

Kissel, C., Laj, C., Rodriguez-gonzalez, A., Perez-torrado, F., Carracedo, J.C., & Wandres (2015). Holocene geomagnetic field intensity variations: Contribution from the low latitude Canary Islands site. *Earth and Planetary Science Letters*, 430, 178–190. doi.org/10.1016/j.epsl.2015.08.005

Kruiver, P.P., Dekkers, M.J., & Heslop, D. (2001). Quantification of magnetic coercivity by the analysis of acquisition curves of isothermal remanent magnetization. *Earth*

and Planetary Science Letters, 189 (3-4), 269–276. doi.org/10.1016/S0012-821X(01)00367-3

Leonhardt, R. (2006). Analyzing rock-magnetic measurements: the RockMagAnalyzer 1.0 software. *Computers & Geoscience*, 32(9), 1420-1431. doi.org/10.1016/j.cageo.2006.01.006

Martínez Ferreras, V., Ariño Gil, E., Gurt Esparraguera, J.M., & Pidaev, S. (2014). The enclosure of Tchingiz Tepe (ancient Termez, Uzbekistan) during the Kushan and Kushan-Sassanian periods. Archaeological stratigraphy and 14C dating analyses. *Iranica Antiqua*, 49, 413–473. doi.org/10.2143/IA.49.0.3009247

Martínez Ferreras, V., Gurt Esparraguera, J.M., Hein, A., Pidaev, S., Rtveladze, E. V., & Bolelov, S.B. (2016). Tableware in the Hellenistic Tradition from the City of Kampyr Tepe in Ancient Bactria (Uzbekistan). *Archaeometry*, 58, 736–764. doi.org/10.1111/arcm.12199

Martínez Ferreras, V., Angourakis, A., Hein, A., Gurt Esparraguera, J.M., Sverchkov, L.M., & Sánchez del Corral, A. (2018). Pottery in Hellenistic tradition from ancient Bactria: The Kurganzol fortress (Uzbekistan, Central Asia). *Journal of Archaeological Science Reports, 21*, 1044–1054. doi.org/10.1016/j.jasrep.2016.11.049

Martínez Ferreras, V., Angourakis, A., Hein, A., Aulinas Juncà, M.; Garcia-Vallés, M.; Gurt Esparraguera, J.M., Ariño Gil, E., Sánchez del Corral, & A., Pidaev, S. (2019). Assessing Hellenistic to nomadic cultural patterns through pottery in ancient Termez, Uzbekistan. *Geoarchaeology,* 34(5), 540–564. doi.org/10.1002/gea.21714

Molina-Cardín, A., Campuzano, S.A., Osete, M.L., Rivero- Montero, M., Pavón-Carrasco, F.J., Palencia- Ortas, A., Martín-Hernández, F., Gómez-Paccard, M., Chauvin, A., Guerrero-Suárez, S., Pérez- Fuentes, J.C., McIntosh, G., Catanzariti, G.,

Sastre-Blanco, J.C., Larrazabal, J., Fernández-Martínez, V.M., Álvarez-Sanchís, J.R., Rodríguez-Hernández, J., Martín-Viso, I., & García I Rubert, D. (2018). Updated Iberian archeomagnetic catalogue: new full vector paleosecular variation curve for the last three millennia. *Geochemistry, Geophysics, Geosystems*, 19, 3637-3656. doi.org/10.1029/2018GC007781.

Nachasova, I., & Burakov, K. (1994). Geomagnetic field intensity from the 3rd century B.C. to the 6th A.D. in Termez (Uzbekistan). *Geomagnetism and Aeronomy (Geomagnetizm i Aeronomiya),* 34, 409–412.

Nachasova, I., & Burakov, K. (1996). Geomagnetic field variations in Central Asia for the last two millenniums: world data analysis. *Geomagnetism and Aeronomy (Geomagnetizm i Aeronomiya),* 35, 844–850.

Nachasova, I., & Burakov, K. (1997). Intensity of the geomagnetic field in Central Asia in 2000 BC–1000 BC. I*zvestiya. Physics of the Solid Earth*, *33*(7), 543-548.

Nagata, T., Arai, Y., K. Momose. (1963). Secular Variation of the Geomagnetic Total Force during the Last 5000 Years. *J. Geophys. Res. 68*, 5277–5282. doi:10.1029/JZ068i018p05277.

O'Reilly, W. (1984). *Rock and Mineral Magnetism.* Glasgow & London: Blackie.

Osete, M.L., Chauvin, A., Catanzariti, G. Jimeno, A., Campuzano, S.A., Benito-Batanero, J.P., Tabernero-Galán, C., & Roperch, P. (2016). New archaeomagnetic data recovered from the study of celtiberic remains from central Spain (Numantia and Ciadueña, 3rd-1st centuries BC). Implications on the fidelity of the Iberian paleointensity database. *Physics of the Earth and Planetary Interiors*, 260, 74–86. doi.org/j.pepi.2016.09.006

Osete, M.L., Molina-Cardín, A., Campuzano, S.A., Aguilella-Arzo, G., Barrachina-Ibañez, A., Falomir-Granell, F., Oliver Foix, A., Gómez-Paccard, M., Martín-

Hernández, F., Palencia-Ortas, A., Pavón-Carrasco, F.J., & Rivero-Montero, M., (2020). Two archaeomagnetic intensity maxima and rapid directional variation rates during the Early Iron Age observed at Iberian coordinates. Implications on the evolution of the Levantine Iron Age Anomaly. *Earth and Planetary Science Letters*, 533, 116047. doi.org/10.1016/J.EPSL.2019.116047

Paterson, G. (2011). A simple test for the presence of multidomain behavior during paleointensity experiments. *Journal of Geophysical Research: Solid Earth*, 116(B10). doi.org/10.1029/2011JB008369

Pavón-Carrasco, F. J., Osete, M. L., Torta, J. M., & De Santis, A. (2014). A geomagnetic field model for the Holocene based on archaeomagnetic and lava flow data. *Earth and Planetary Science Letters*, 388, 98–109. doi.org/10.1016/j.epsl.2013.11.046

Petersen, N., & Petersen, K. (2008). Comparison of the temperature dependence of irreversible and reversible magnetization of basalt samples. *Physics of the Earth and Planetary Interiors*, 169, 89–91. doi.org/10.1016/0031-9201(77)90108-X

Rivero-Montero, M., Gómez-Paccard, M., Kondopoulou, D., Tema, E., Pavón-Carrasco, F.J., Aidona, E., Campuzano, S.A., Molina-Cardín, A., Osete, M.L., Palencia-Ortas, A., Martín-Hernández, F., Rubat-Borel, F., & Venturino, M. (2021a). Geomagnetic field intensity changes in the central Mediterranean between 1500 BCE and 150 CE: implications of the LIAA evolution. *Earth and Planetary Science Letters*, 557,116732. doi.org/10.1016/j.epsl.2020.116732.

Rivero-Montero, M., Gómez-Paccard, M., Pavón-Carrasco, F.J., Cau-Ontiveros, M.A., Fantuzzi, L., Martín-Hernández, F., Palencia-Ortas, A., Aidona, E., Tema, E., Kondopoulou, D., Mas-Florti, C. & Ramon-Torres, J. (2021b). Refining geomagnetic field intensity changes in Europe between 200 CE and 1800 CE. New data from the Mediterranean region. *Physics of the Earth and Planetary Interiors*,

317, 106749. doi.org/10.1016/j.epsl.2020.116732.

Roberts, A.P., Tauxe, L., Heslop, D., Zhao, X., & Jiang, Z. (2018). A Critical Appraisal of the "Day" Diagram. *Journal of Geophysical Research: Solid Earth*, 123, 2618–2644. doi.org/10.1002/2017JB015247

Rogers, J., J. M. W. Fox, & Aitken, M. J. (1979). Magnetic anisotropy in ancient pottery. *Nature*, 277(5698), 644–646. doi.org/10.1038/277644a0

Schnepp, E., Thallner, D., Arneitz, P., & Leonhardt, R. (2020). New archeomagnetic secular variation data from Central Europe, II: Intensities. *Physics of the Earth and Planetary Interiors*, 309, 106605. doi.org/10.1016/j.pepi.2020.106605

Shaar, R., Ben-Yosef, E., Ron, H., Tauxe, L., Agnon, A., & Kessel, R. (2011). Geomagnetic field intensity: How high can it get? How fast can it change? Constraints from Iron Age copper slag. *Earth and Planetary Science Letters*, 301, 297–306. doi.org/10.1016/j.epsl.2010.11.013

Shaar, R., Tauxe, L., Ron, H., Ebert, Y., Zuckerman, S., Finkelstein, I., & Agnon, A. (2016). Large geomagnetic field anomalies revealed in Bronze to Iron Age archeomagnetic data from Tel Megiddo and Tel Hazor, Israel. *Earth and Planetary Science Letters*, 442, 173–185. doi.org/10.1016/j.epsl.2016.02.038

Shaar, R., Tauxe, L., Goguitchaichvili, A., Devidze, M., & Licheli, V. (2017). Further evidence of the Levantine Iron Age geomagnetic anomaly from Georgian pottery. *Geophysical Research Letters*, 44(5), 2229–2236. doi.org/10.1002/2016GL071494

Sverchkov, L. (2013). *Kurganzol-Krepost Aleksandra na yugye Uzbekistana.* Tashkent, Uzbekistan: SMI-ASIA.

Tauxe, L. (1998). *Paleomagnetic principles and Practise.* Dordrecht, Netherlands: Kluwer Academic Publishers.

Tauxe, L., Staudigel, H. (2004). Strength of the geomagnetic field in the Cretaceous

Normal Superchron: new data from submarine basaltic glass of the Troodos *Ophiolite*. *Geochem. Geophys. Geosyst. 5* (2), Q02H06, doi:10.1029/2003GC000635.

Tema, E., & Lanos, P. (2021). New Italian directional and intensity archaeomagnetic reference curves for the past 3000 years: insights on secular variation and implications on dating. *Archaeometry*. doi.org/10.1111/arcm.12603

Thébault, E., & Gallet, Y., 2010. A bootstrap algorithm for deriving the archeomagnetic field intensity variation curve in the Middle East over the past 4 millennia BC. *Geophysical research letters*, 37(22).

Thellier, E., & Thellier, O. (1959). Sur l'intensité du champ magnétique terrestre dans le passé historique et géologique. *Annales de Géophysique*, 15, 285–376.

Tsantini, E., Martínez Ferreras, V., Ariño Gil, E., Gurt Esparraguera, J.M.; Pidaev, S.R. (2016), Pottery production in the Buddhist communities in Central Asia: The Kushan-Sassanian pottery workshop of Kara Tepe (Termez, Uzbekistan). *Archaeometry 58(1),* 35–56. doi. 10.1111/arcm.12161

Troyano, M., Gallet, Y., Genevey, A., Pavlov, V., Fournier, A., Lagroix, F., Niyazova, M., & Mirzaakhmedov, D. (2021). Analyzing the geomagnetic axial dipole field moment over the historical period from new archeointensity results at Bukhara (Uzbekistan, Central Asia). *Physics of the Earth and Planetary Interiors, 310,* 106633. doi.org/10.1016/j.pepi.2020.106633

Usoskin, I.G., Gallet, Y., Lopes, F., Kovaltsov, G.A., & Hulot, G. (2016). Solar activity during Holovene: the Hallstatt cycle and its consequence for grand minima and maxima. *Astronomy and Astrophysics, 587,* A150. doi.org/10.1051/0004-6361/201527295

Zijderveld, J.D.A. (1967). AC Demagnetization of Rocks: Analysis of Results. *Methods*

in Palaeomagnetism, pp. 254-286. Elsevier, New York.

Figure captions

Figure 1. a) Location of the archaeological sites from where the studied materials were recovered. b) Picture of Kampyr Tepe archaeological site. c) Pictures of some of the ceramic assemblages studied.

Figure 2. Representative rock magnetic results. The three different cities studied in this work are represented in different colours: blue, Kampyr Tepe; orange, Kurganzol; purple, Termez. a) Magnetization versus temperature (MT) thermomagnetic curves. Three different colours correspond to the three groups obtained by studying Curies temperatures. b) Susceptibility versus temperature (χT) curves. c) Hysteresis loops measured up to 500 mT. d) Day plot (Day et al., 1977) with SD-MD mixing curves for magnetite (Dunlop, 2002) showing the results obtained for all the studied samples. e) IRM acquisition curve and separation into three components to obtain the best fit (Kruiver et al., 2001). f) Typical example of an alternating field (AF) demagnetization experiment from 5 mT to 120 mT.

Figure 3. Arai diagrams (Nagata, Arai and Momose, 1963) (x axis normalized by total pTRM) together with Zijderveld (Zijderveld, 1967) plots for representative specimens for (a) Kurganzol, (b) Kampyr Tepe's Pottery Workshop, (c) Low city, (d) Citadel and (e, f, g, h, i, j, k, l) Termez. The initial natural remanent magnetization (NRM), the archeointensity obtained before (H) and after (H_a) the TRM anisotropy correction and the

quality factor *q* defined by Coe et al. (1978) are indicated.

Figure 4. Quality parameters at the specimen level obtained after the TRM anisotropy correction. N, number of steps for the slope calculation; f, fraction of NRM used for the slope calculation; g, gap factor; q, quality factor; MAD, maximum angle of deviation (in º); DANG, deviation angle (in º); β, ratio of the standard error of the slope to the absolute value of the slope; k, curvature parameter (see main text for details).

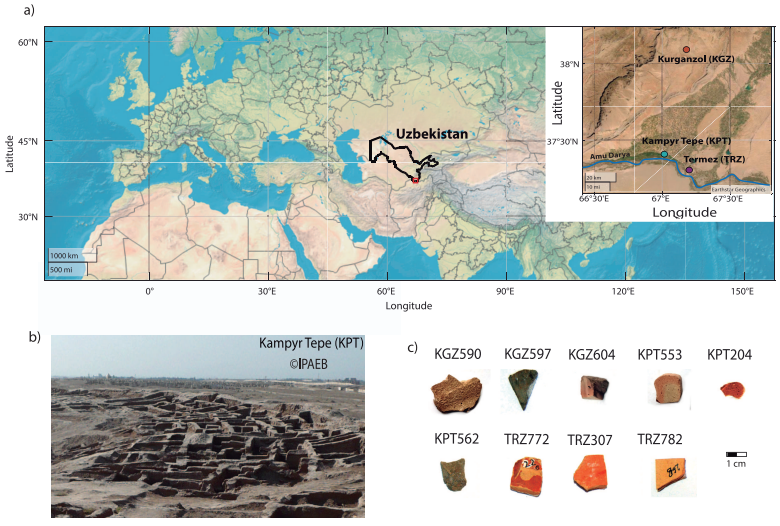
Figure 5. New archeointensity results obtained for South Uzbekistan (Kurganzol, orange dots; Kampyr Tepe, blue dots; Termez, purple dots) and the new PSV curves proposed here for central Asia between 600 BCE and 600 CE (orange line), plotted with its 2-sigma error band (shaded area). Also, the prediction of different global geomagnetic field models has been represented: SHA.DIF.14k (Pavón-Carrasco et al., 2014), SHAWQ Iron Age (Osete et al., 2020), SHAWQ.2k (Campuzano et al., 2019), ARCH10k (Constable et al., 2016), CALS10k.2 (Constable et al., 2016). The data, curves and models are all relocated to Termez coordinates (37.3º N, 67.2º E).

Figure 6. Comparison between the virtual axial dipole moment (VADM) local values derived from individual archeointensities and the dipole moment (DM, coloured lines) and axial dipole moment (ADM, dashed coloured lines) variation derived from different global geomagnetic field reconstructions: GMAG (VADM values, Usoskin et al., 2016), SHA.DIF.14k (Pavón-Carrasco et al., 2014), SHAWQ Iron Age (Osete et al., 2020), SHAWQ.2k (Campuzano et al., 2019), CALS10k.2 (Constable et al., 2016).

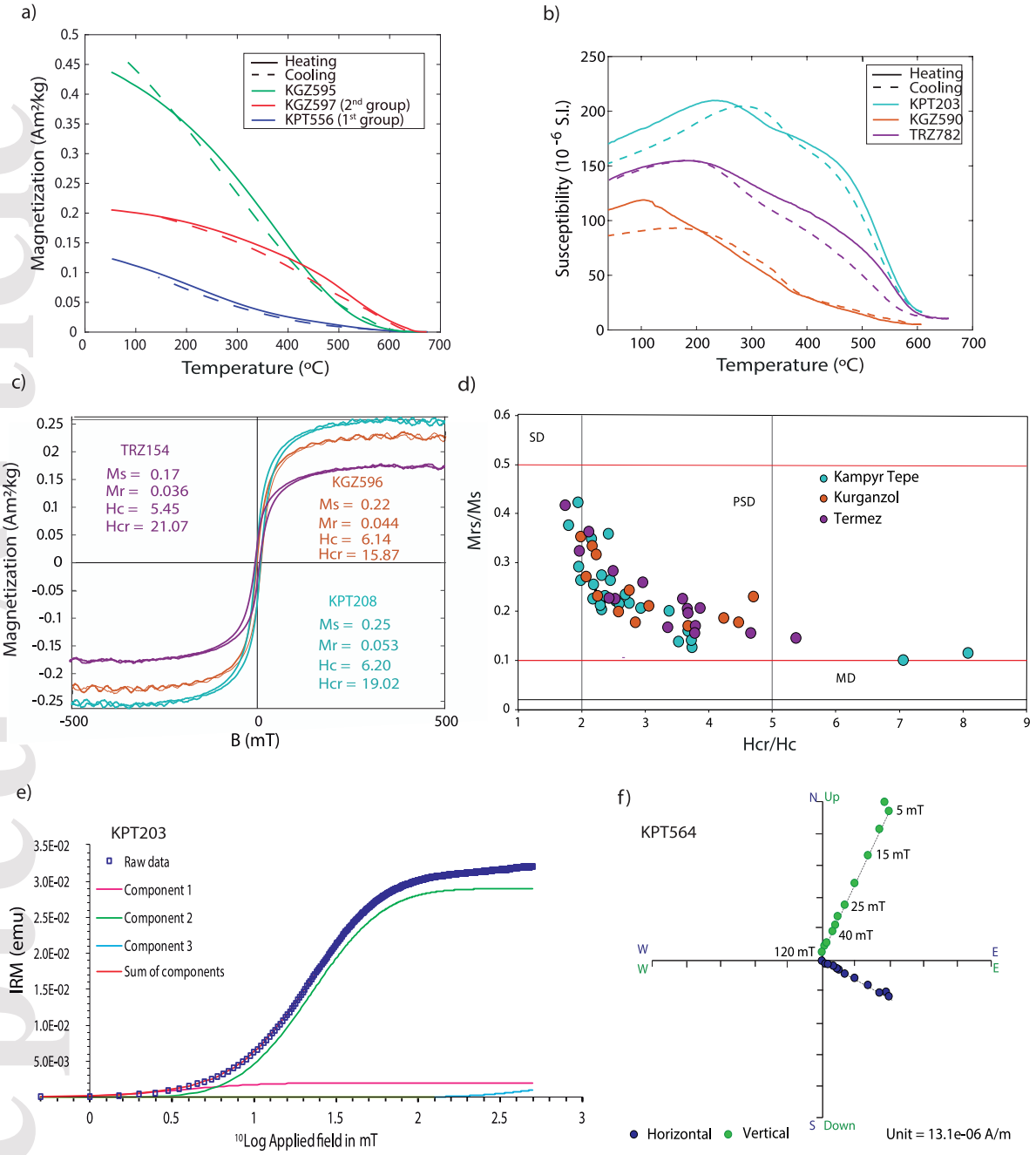
Figure 7. Comparison between the virtual axial dipole moment (VADM) local values available for different regions. New data from this study are showed as purples dots. Grey dots represent low quality data and coloured circles high quality previous data (see text for further details).

Figure 8. Comparison between the secular variations per century (SV) calculated for the different regions analysed in Figure 7. Error bars correspond to the standard deviation of the PSV curves.

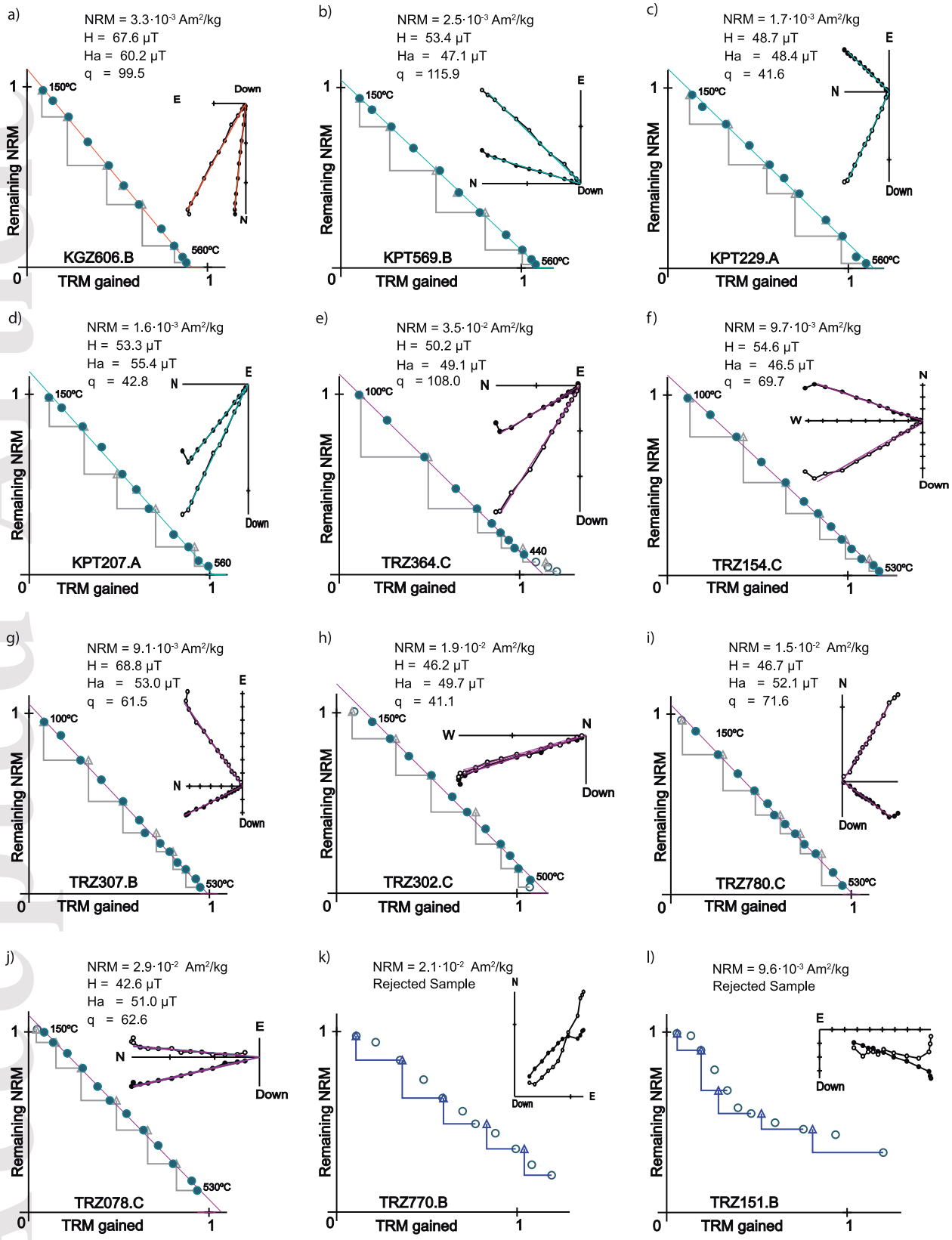
Accepted Article



This article is protected by copyright. All rights reserved.

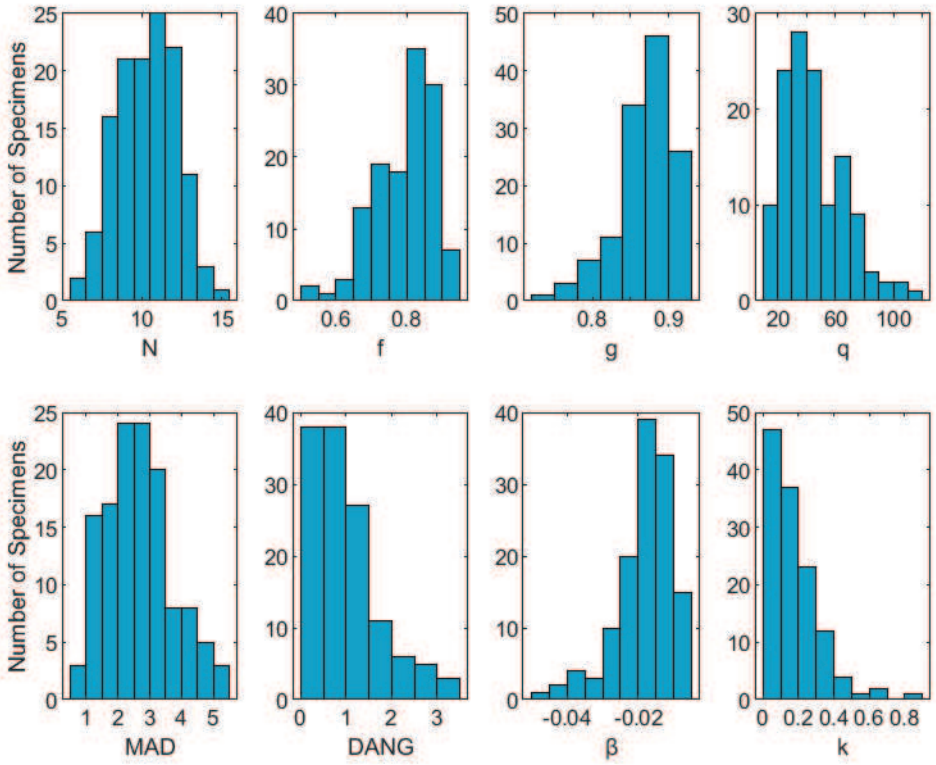


This article is protected by copyright. All rights reserved.



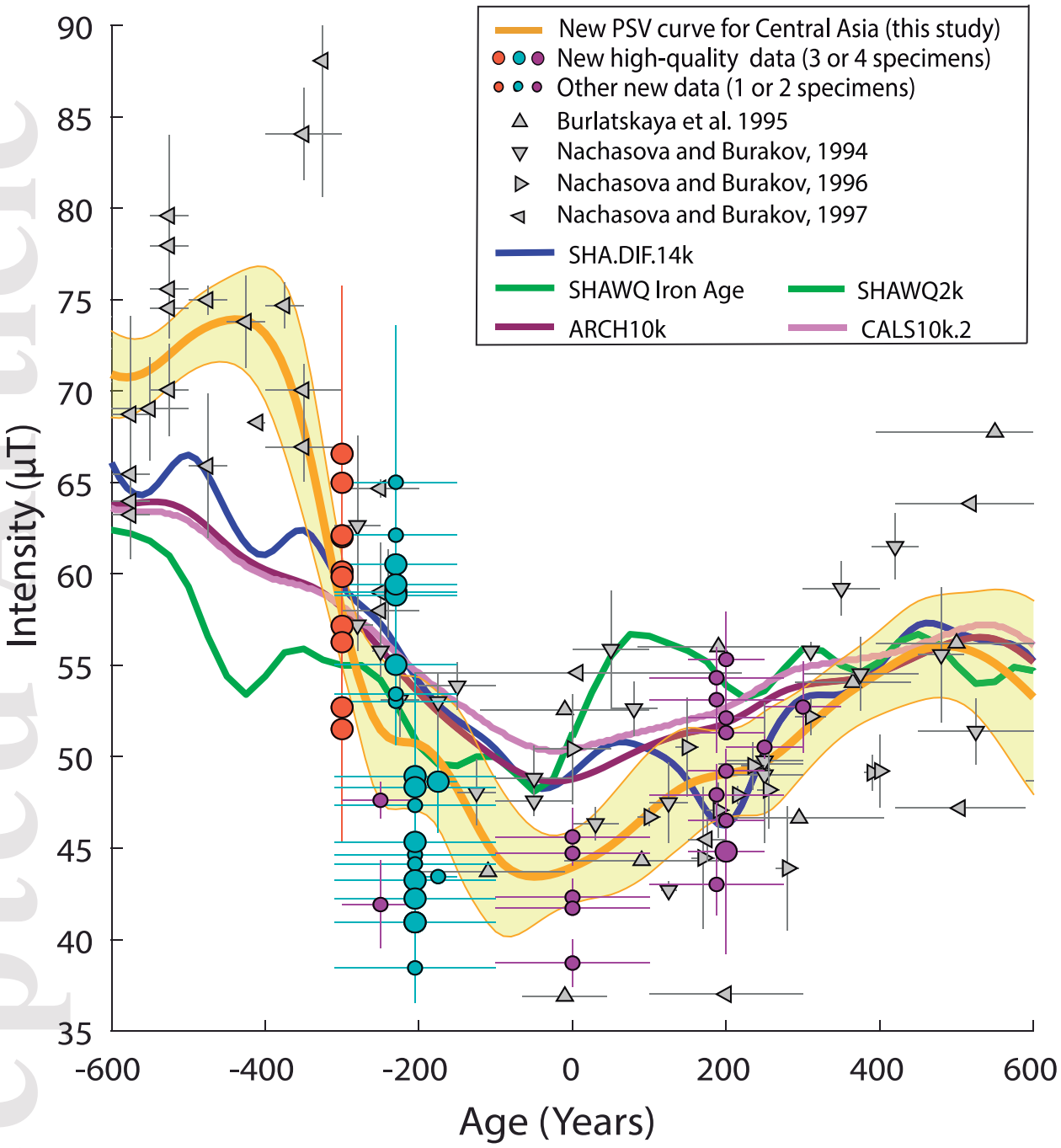
This article is protected by copyright. All rights reserved.

Accepted Article



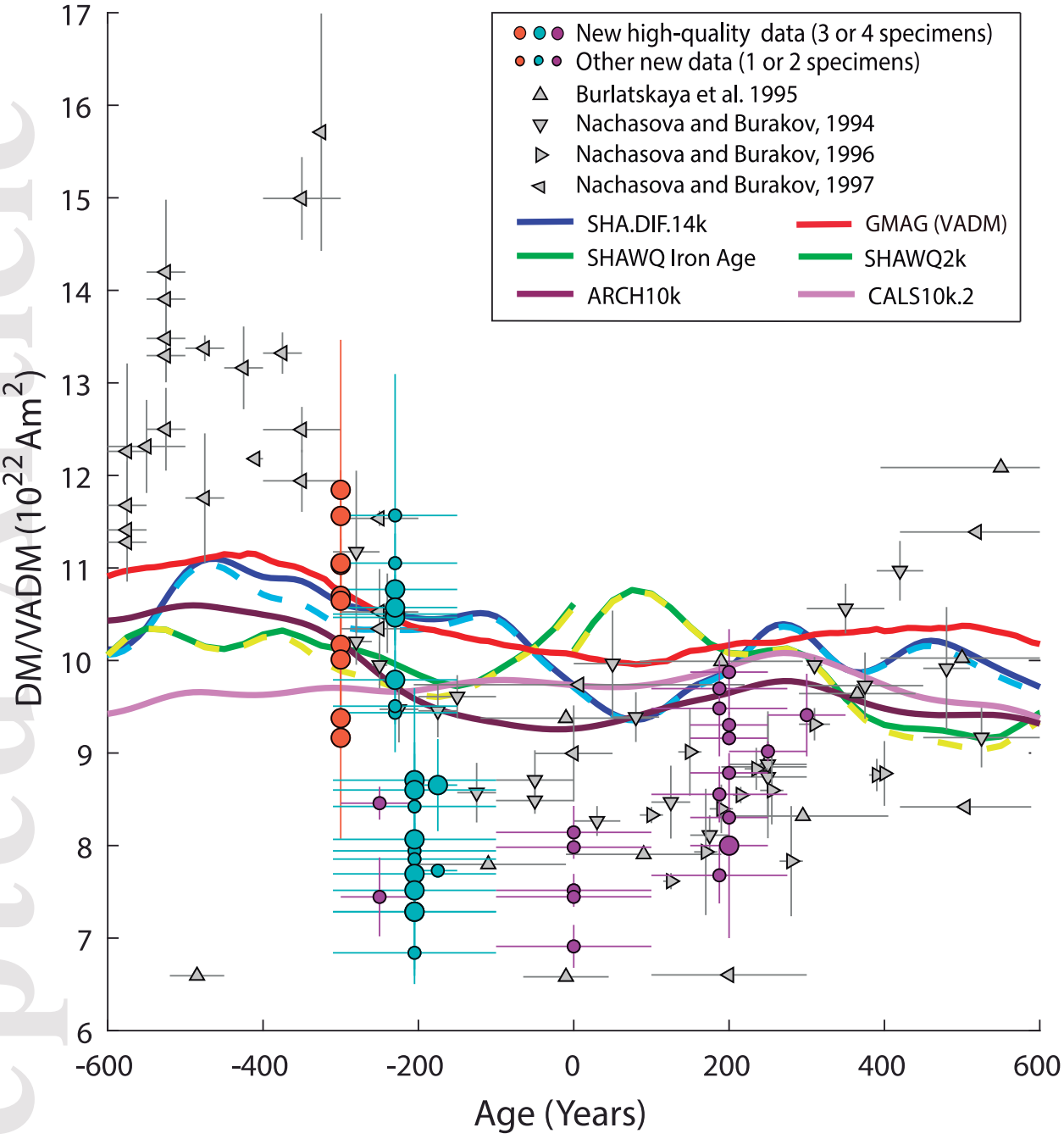
This article is protected by copyright. All rights reserved.

Accepted Article



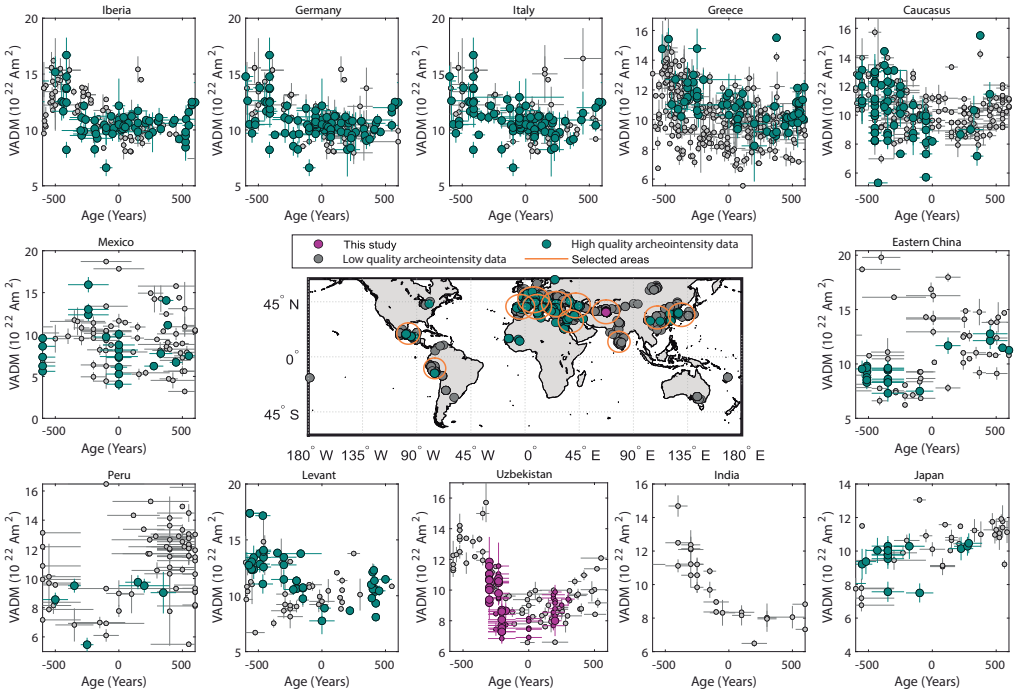
This article is protected by copyright. All rights reserved.

Accepted Article

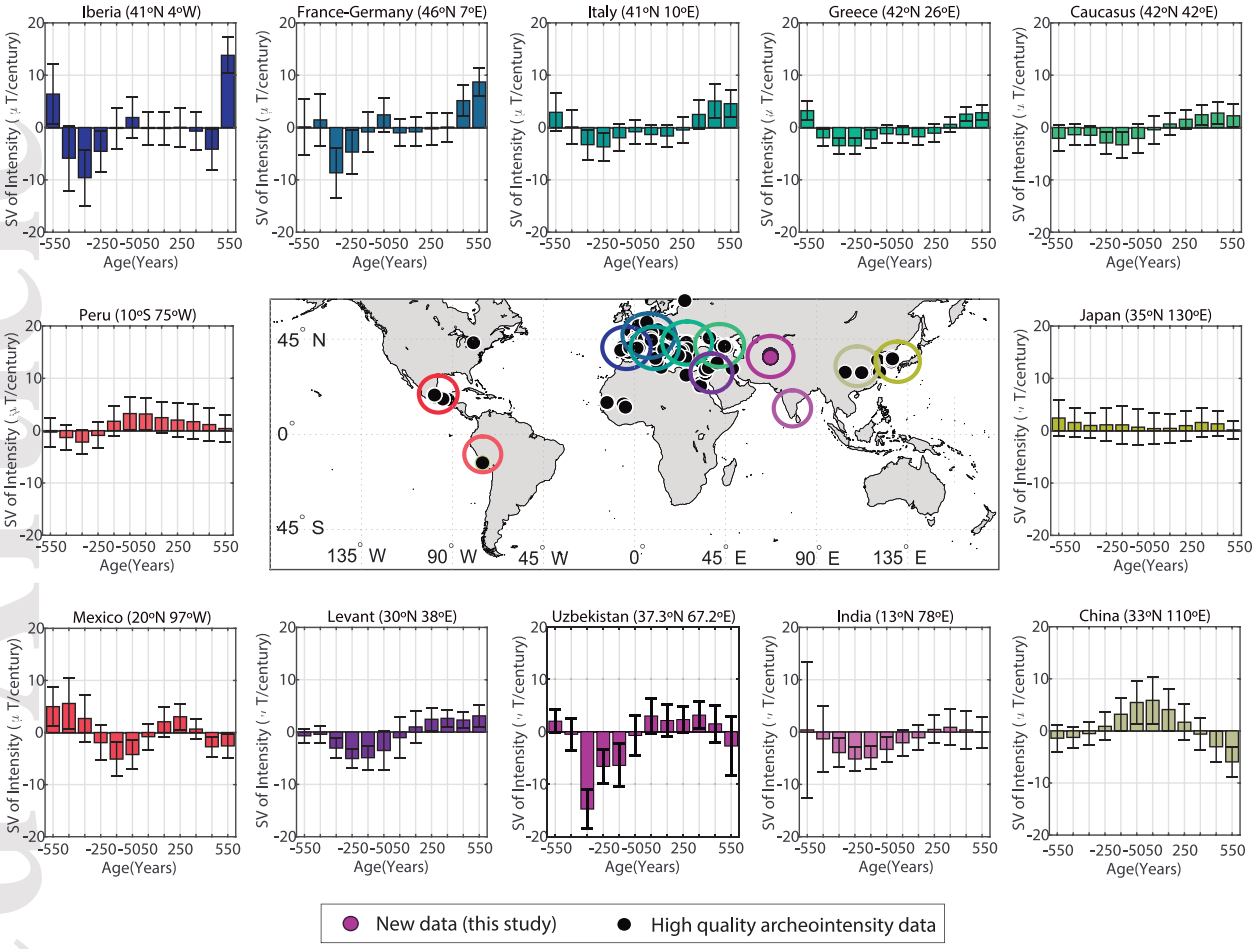


This article is protected by copyright. All rights reserved.

Accepted Article



This article is protected by copyright. All rights reserved.



This article is protected by copyright. All rights reserved.

1. Kurganzol (Lat: 38.09 ºN; Lon: 67.18 ºE)				
Sample	**n**	**H_{ac}**	**H_{Reloc}**	**VADM**
a) Military Fortress: 310-290 BCE				
KGZ599	4	62.6 ± 4.2	62.0	11.0 ± 0.7
KGZ602	4	67.2 ± 9.2	66.6	11.8 ± 1.6
KGZ604	4	65.6 ± 2.8	65.0	11.6 ± 0.5
KGZ606	4	57.7 ± 5.2	57.2	10.2 ± 0.9
KGZ607	4	52.0 ± 6.2	51.5	9.2 ± 1.1
KGZ603	4	53.2 ± 1.8	52.7	9.4 ± 0.3
KGZ593	3	62.7 ± 1.5	62.1	11.1 ± 0.3
KGZ594	3	60.7 ± 2.5	60.1	10.7 ± 0.4
KGZ595	3	60.4 ± 1.6	59.8	10.6 ± 0.3
KGZ596	3	56.8 ± 3.5	56.3	10.0 ± 0.6
Mean			***59.3 ± 4.9***	***10.6 ± 0.9***
2. Kampyr Tepe (Lat: 37.41 ºN; Lon: 67.02 ºE)				
Sample	**n**	**H_{ac}**	**H_{Reloc}**	**VADM**
b) Citadel: 310-150 BCE				
KPT237	4	55.1 ± 1.8	55.0	9.8 ± 0.3
KPT205	4	59.1 ± 1.0	59.0	10.5 ± 0.2
KPT207	3	58.9 ± 0.5	58.8	10.5 ± 0.1
KPT203	3	60.6 ± 3.4	60.5	10.8 ± 0.6
KPT208	3	59.5 ± 2.0	59.4	10.6 ± 0.4
KPT242	2	53.1 ± 0.7	53.0	9.4 ± 0.1
KPT240	2	62.2 ± 11.5	62.1	11.1 ± 2.0
KPT206	1	65.1	65.0	11.6
KPT241	1	53.5	53.4	9.5
Mean			***58.5 ± 4.0***	***10.4 ± 0.7***
c) Low City: 200-150 BCE				
KPT229	3	48.7 ± 2.8	48.6	8.7 ± 0.5
KPT228	1	43.5	43.4	7.7
Mean			***46.0 ± 3.7***	***8.2 ± 0.7***
d) Pottery Workshop: 310-100 BCE				
KPT553	4	41.0 ± 3.9	40.9	7.3 ± 0.7
KPT556	4	43.3 ± 3.1	43.2	7.7 ± 0.6
KPT564	4	49.0 ± 5.6	48.9	8.7 ± 1.0
KPT557	3	42.3 ± 1.2	42.2	7.5 ± 0.2
KPT558	3	41.0 ± 3.5	40.9	7.3 ± 0.6
KPT569	3	48.4 ± 2.9	48.3	8.6 ± 0.5
KPT570	3	45.4 ± 1.7	45.3	8.1 ± 0.3
KPT567	2	47.4 ± 3.2	47.3	8.4 ± 0.6
KPT561	2	38.5 ± 1.9	38.4	6.8 ± 0.3
KPT560	1	44.7	44.6	7.9
KPT563	1	44.2	44.1	7.9
Mean			***44.0 ± 3.3***	***7.8 ± 0.6***
3. Termez (Lat: 37.30 ºN; Lon: 67.20 ºE)				
Sample	**n**	**H_{ac}**	**H_{Reloc}**	**VADM**
a) Alluvial Plain. AC2 - SU33: 300-200 BCE				

Accepted Article

This article has been accepted for publication and undergone full peer review but has not been through the copyediting, typesetting, pagination and proofreading process, which may lead to differences between this version and the Version of Record. Please cite this article as doi: 10.1029/2021JB022011.

This article is protected by copyright. All rights reserved.

TRZ363	2	41.9 ± 2.4	41.9	7.4 ± 0.4
TRZ364	2	47.6 ± 1.0	47.6	8.5 ± 0.2
Mean			***44.8 ± 4.0***	***8.0 ± 0.8***
b) Alluvial Plain: AC1 - SU 12: 100 BCE-100 CE				
TRZ153	2	42.3 ± 1.0	42.3	7.5 ± 0.2
TRZ154	2	45.6 ± 1.6	45.6	8.1 ± 0.3
TRZ155	2	44.7 ± 0.0	44.7	8.0 ± 0.0
TRZ716	2	38.7 ± 1.3	38.7	6.9 ± 0.2
TRZ717	1	41.7	41.7	7.4
Mean			***42.6 ± 2.7***	***7.6 ± 0.5***
c) Tchingiz Tepe: *RC - SU18: 100-275 CE*				
TRZ297	2	43.0 ± 1.7	43.0	7.7 ± 0.1
TRZ780	2	53.1 ± 2.9	53.1	9.5 ± 0.5
TRZ781	2	47.9 ± 1.7	47.9	8.6 ± 0.3
TRZ782	2	54.3 ± 0.4	54.3	9.7 ± 0.1
Mean			***49.6 ± 5.2***	***8.9 ± 0.9***
d)* Tchingiz Tepe: *RC - SU21: 150-250 CE				
TRZ302	3	44.8 ± 5.6	44.8	8.0 ± 1.0
TRZ179	2	46.5 ± 0.5	46.5	8.3 ± 0.1
TRZ181	2	55.3 ± 2.6	55.3	9.9 ± 0.5
TRZ776	2	52.1 ± 0.8	52.1	9.3 ± 0.1
TRZ770	1	49.2	49.2	8.8
TRZ772	1	51.3	51.3	9.2
Mean			***49.9 ± 3.8***	***8.9 ± 0.7***
e)* Tchingiz Tepe: *RC - SU5: 250-350 CE				
TRZ078	2	52.7 ± 2.5	52.7	9.4 ± 0.4
f)* Tchingiz Tepe: *RC - SU25: 200-300 CE				
TRZ307	2	50.5 ± 0.6	50.5	9.0 ± 0.1

Table 1. Sample, fragment's name; n, number of specimens used to calculate the mean intensity; $H_{ac,}$ intensity and standard deviation, s.d., (in μT) obtained considering both the TRM anisotropy and cooling rate corrections; H_{Reloc} intensity and s.d. (in μT) relocated to Termez coordinates; VADM, Virtual Axial Dipole Moment and corresponding uncertainty (in 10^{22} Am^2).

This article is protected by copyright. All rights reserved.